Effect of cooling rate and chemistry on mechanical properties of Ti-V HSLA plate steels

Seyed Reza Jafarpour Rezaei[1*], *Charles W.* Siyasiya[1], *Joseph* Moema[2], and *Zheng-hua* Tang[3]

[1]Department of Materials Science & Metallurgical Engineering, University of Pretoria, South Africa
[2]Advanced Material Division, Mintek, South Africa
[3]Department of Materials Science & Engineering, University of Sichuan, China

Abstract. High strength low alloy (HSLA) steels are known for their superior mechanical properties, which are achieved through alloying elements and controlled hot rolling. In this work, the effect of cooling rate and alloying elements on the final microstructure and mechanical properties of Ti-V HSLA microalloyed steels were investigated. The Gleeble 1500TM ™ was used to simulate the plate rolling process. The samples were cooled to room temperature using two different cooling rates to simulate the 16 and 30mm thick plate cooling patterns in the alloy. Increasing the cooling rate and amount of carbon equivalent promoted acicular ferrite and bainite transformation, and also led to the decrease in grain size. Consequently, both the yield strength and UTS increased with increasing cooling rate with a slight drop in uniform elongations.

1 Introduction

One of the major environmental and societal challenges for the 21st century is the global increase in urban pollution. Naturally, this is related to the increase in transport vehicles on the road. Increasing consumption of petroleum results in increasing emissions of greenhouse gases and adversely impacts on environment. Some of the environmental effects of greenhouse gases are global warming, sea level rise, agricultural impact, and effects on aquatic systems [1,2]. Strategies proposed to address these effects encompasses the optimization of product design, the integration of lightweight materials, the practice of downgauging, and the adoption of advanced manufacturing techniques [3]. These approaches are inherently interrelated, with their effectiveness largely influenced by the specific characteristics of the lightweight materials employed to manufacture them. Despite ongoing advancements, steel continues to be the primary engineering alloy in automotive and structural applications due to its cost-effectiveness, mechanical performance, ease of fabrication, recyclability, and versatility [4, 5]. Stakeholders across the automotive value chain including manufacturers, material developers, and component suppliers have long invested in the advancement and implementation of both ferrous and nonferrous lightweight solutions. Central to these efforts is the development of High-Strength Low-Alloy (HSLA)

* Corresponding author: rezajafarpour2010@gmail

© The Authors, published by EDP Sciences. This is an open access article distributed under the terms of the Creative Commons Attribution License 4.0 (https://creativecommons.org/licenses/by/4.0/).

steels, whose microstructures can be tailored to achieve exceptional mechanical properties, which includes high tensile strength and excellent ductility. These steels allow for the reduction in structural component thickness referred to as downgauging without compromising performance, thereby contributing to lighter vehicles and cost savings [6, 7].

The mechanical properties of microalloyed steels are significantly influenced by several factors such as grain refinement, solid-solution strengthening, dislocation density, precipitation hardening, and ferrite grain size. [8]. A fine and uniform ferrite grain size in the final microstructure is preferred, as it enhances both strength and toughness [9, 10]. To achieve this, the thermomechanical controlled process (TMCP) is commonly employed to refine the microstructure of HSLA steels. Process parameters including amount of deformation, rolling temperature, cooling pattern, cooling rate, and coiling temperature have a direct impact on the microstructure and mechanical properties. Among these, the cooling rate plays a critical role in determining the final microstructure and mechanical behavior [11, 12]. Bhattacharya et al. [13] demonstrated that the cooling rate plays a crucial role in phase transformations, significantly influencing the final microstructure. The cooling rate influences the phase transformation of the precipitates and the ferrite grain size, both of which are crucial in determining the final mechanical properties [14].

This study investigates the influence of cooling rate and alloy chemistry on the microstructure and mechanical properties of high Ti-V HSLA steel, using simulated cooling patterns corresponding to 16- and 30-mm plate thicknesses.

2 Materials and experimental method

2.1 Materials

The steels in this study were produced by vacuum induction melting using high-purity raw materials, and their chemical compositions are listed in Table 1. The alloys were cast into ingots, from which cylindrical specimens (10 mm in diameter and 15 mm in height) were machined for the TMCP simulations using the Gleeble 1500 machine.

Table 1. Chemical composition of tested steels (%mass)

Alloy	C	Si	Mn	V	Ti	S	P	N	Cr	Fe	C_{eq}
A1	0.14	0.44	1.62	0.13	0.10	0.02	0.017	0.005	0.62	Bal.	0.560
A2	0.15	0.45	1.63	0.067	0.10	0.018	0.017	0.004	0.64	Bal.	0.563
A3	0.1	0.30	1.11	0.06	0.05	0.007	0.010	0.006	0.65	Bal.	0.427

2.2 Experimental method

Figure 1 shows the schematic diagram of the TMCP simulation. Samples were reheated to 1150˚C at a rate of 10˚C/s, held for 300 s, and then cooled to the deformation temperatures at the same rate. They were then held for 10 s before undergoing isothermal compression tests in five passes at 1100, 1075, 1050, 1000 and 975˚C, with applied strains of 0.2, 0.2, 0.2, 0.15, and 0.15 respectively, at a strain rate of 2.5 s^{-1}. After final deformation, the specimens were continuously cooled to room temperature using two distinct cooling patterns, simulating the conditions for the 16- and 30-mm thick plates [15].

The specimens sectioned along the deformation axis were grinded, polished and etched with 4% Nital solution, and the microstructures were examined using an Olympus BX51MTM optical microscope. Nanoscale precipitates were characterized by transmission

electron microscopy (TEM) using the carbon replica extraction method. Polished and etched surfaces were carbon-coated in a vacuum evaporator, followed by selective dissolution of the matrix to isolate the precipitates. The resulting carbon films were transferred onto copper grids and analyzed using a JEOL 2100F Field-Emission TEM (200 kV) equipped with an EDS detector for compositional analysis.

Mechanical properties were assessed using Vickers hardness machine and profilometry-based indentation plastometry (PIP). Hardness was determined from the average of fifteen measurements taken along the sample center. The tensile properties were obtained using profilometry-based indentation plastometry (PIP), which correlates indentation response with bulk tensile behaviour. The yield strength, ultimate tensile strength (UTS), and uniform elongation were extracted through analytical modelling of the PIP data [16].

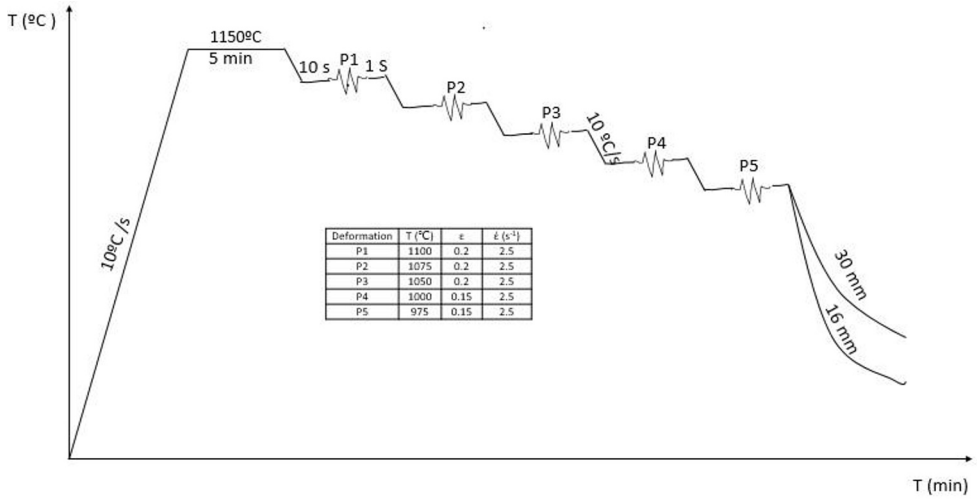

Deformation	T (ºC)	ε	$\dot{\varepsilon}$ (s^{-1})
P1	1100	0.2	2.5
P2	1075	0.2	2.5
P3	1050	0.2	2.5
P4	1000	0.15	2.5
P5	975	0.15	2.5

Fig. 1. Thermomechanical process schedule.

3 Results and discussion

3.1 Microstructure

The microstructure of the examined steels after cooling are shown in Figure 2. Microstructural analysis reveals that at lower cooling rates, polygonal ferrite (PF) and pearlite (P) are the predominant phases across all tested steels. As the cooling rate increases, these phases remain dominant in alloy A3. However, in alloys A1 and A2 with slightly higher carbon content, acicular ferrite (AF) and bainite (B) begin to form in addition to polygonal ferrite and pearlite, (Figures 2d and 2e). Furthermore, noticeable polygonal ferrite grain refinement occurred in all samples with decreasing cooling temperature (Figure 3). This is due to the increasing cooling rate and, therefore the driving force for phase transformation. In other words, the critical nucleation size of the nuclei and activation energy decrease, resulting in a higher nucleation rate. The enhanced nucleation rate limits grain growth due to impingement grains, ultimately promoting the refinement of grains [17].

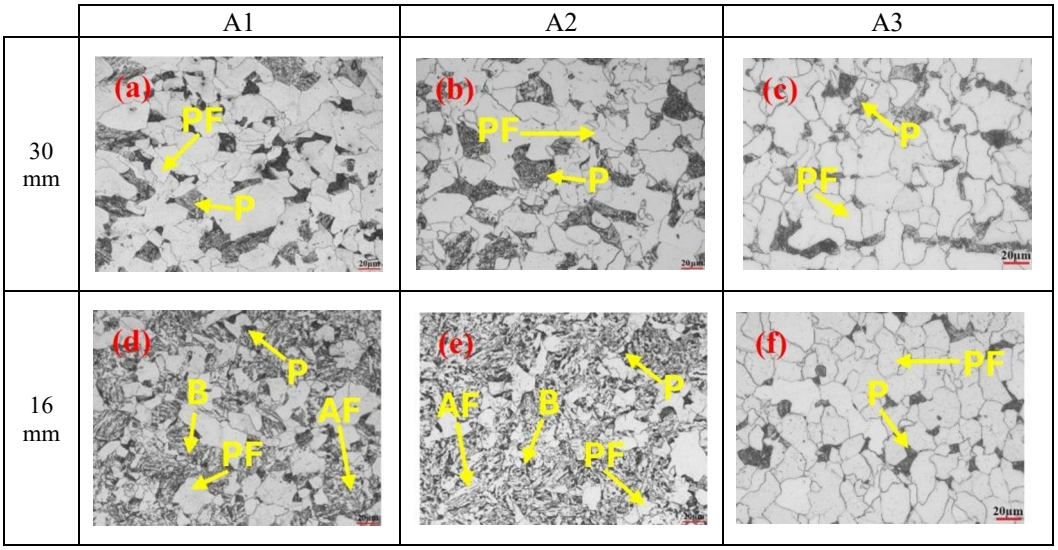

Fig. 2. Optical micrograph of investigated steels after cooling.

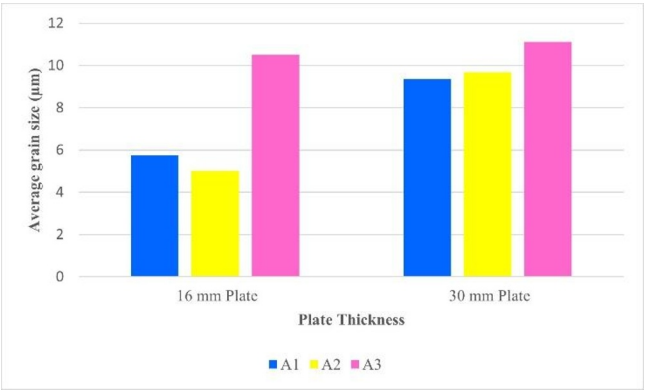

Fig. 3. Average of grain size of specimens after cooling.

3.2 Precipitation

Precipitation behavior was simulated using the Thermo-Calc software, Figure 4. The precipitates can be classified into three distinct groups: (i) coarse precipitates that form in the molten state (e.g., TiN), (ii) precipitates that form in austenite during slab reheating (e.g., $Ti_4C_2S_2$), and (iii) fine precipitates that form at low temperatures during the austenite-to-ferrite transformation (e.g., VC).

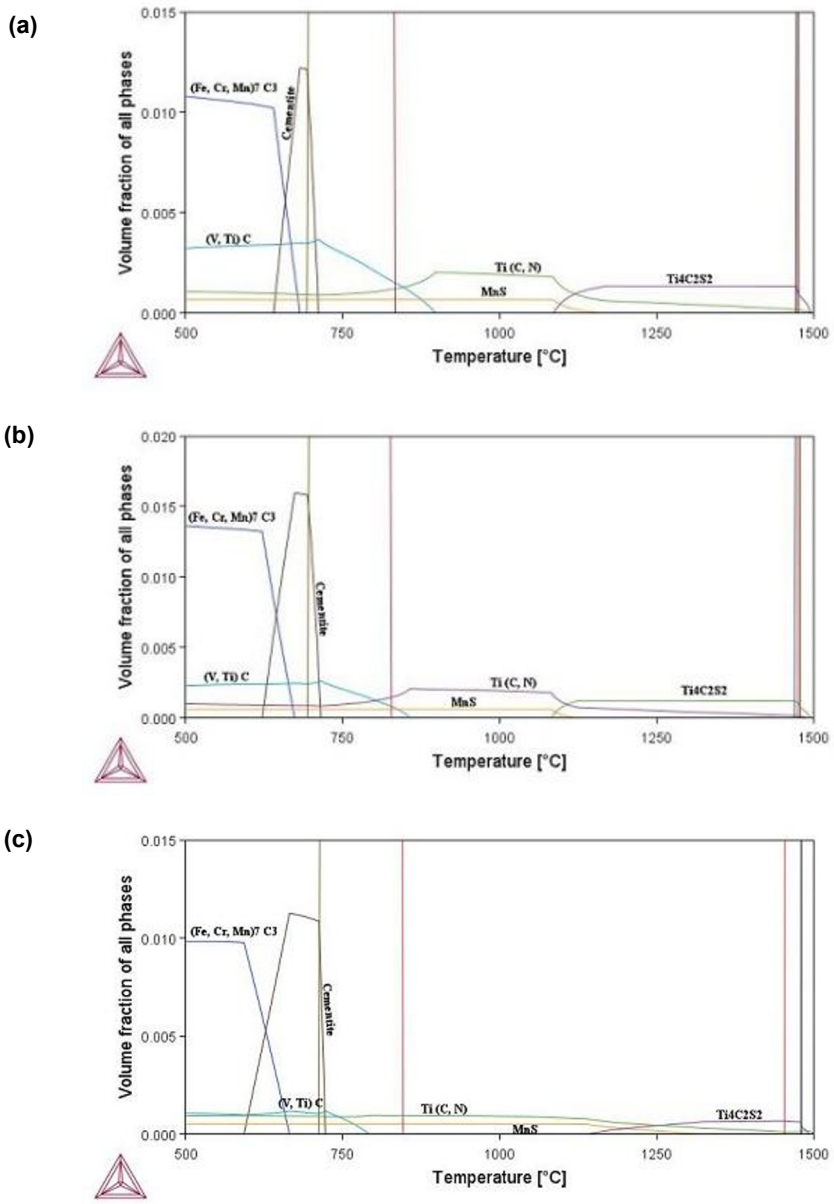

Fig. 4. Thermo-Calc prediction of precipitate formation for steels, (a) A1, (b) A2, and (c) A3.

Figure 5 illustrates the morphology and types of precipitates observed in alloy A1 after reheating. The SEM-EDS analysis confirmed the presence of stable TiN, MnS, and $Ti_4C_2S_2$ phases at the reheating temperature of 1150°C, which is consistent with Thermo-Calc prediction.

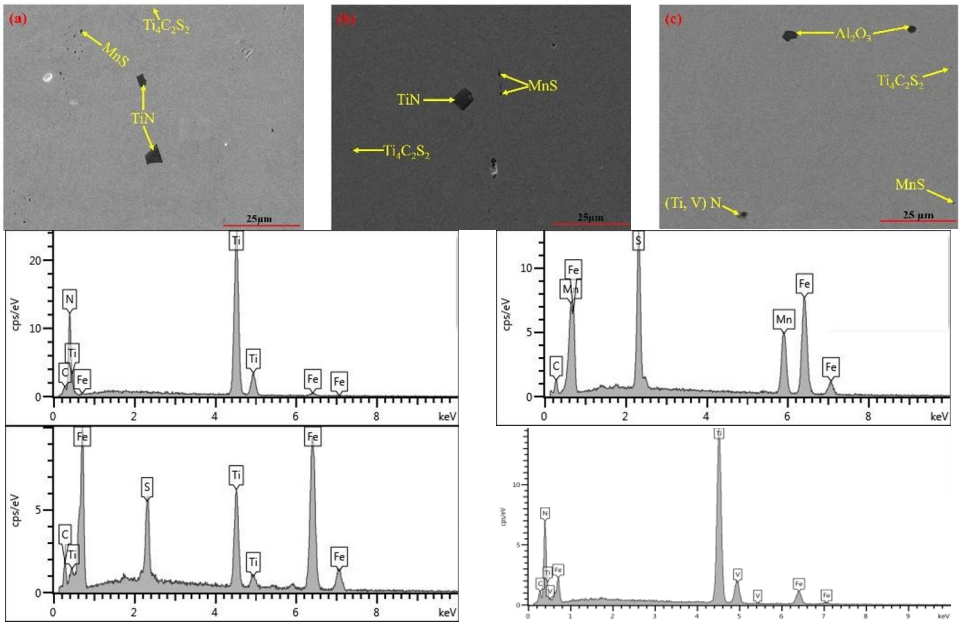

Fig. 5. SEM-SE images showing precipitate morphology and types, along with corresponding EDS spectra, after reheating at 1150°C for 300 s for steels: (a) A1, (b) A2, and (c) A3.

Figure 6 presents the TEM carbon replica images of the precipitates for A1, and Figure 7 illustrates their average sizes after cooling. It was found that the precipitate size in alloy A3 at both cooling rates was smaller compared to A1 and A2. Additionally, an increase in the cooling rate led to a reduction in precipitate size due to several mechanisms. The involved mechanisms include enhanced solute supersaturation, altered phase transformation, and refined microstructural features, which collectively contribute to reduction in precipitate size [18, 19]. The relationships between the size, D_p, and the volume fraction, V_p, of precipitates and the cooling rate are, respectively, were given by Eq.1 and 2 [20]:

$$D_P = C \times \vartheta_c^{-n} \quad (1)$$

$$V_P = A/exp\,(B \times \vartheta_c) \quad (2)$$

Where υ_c is the cooling rate, A, B, C and n are constant.

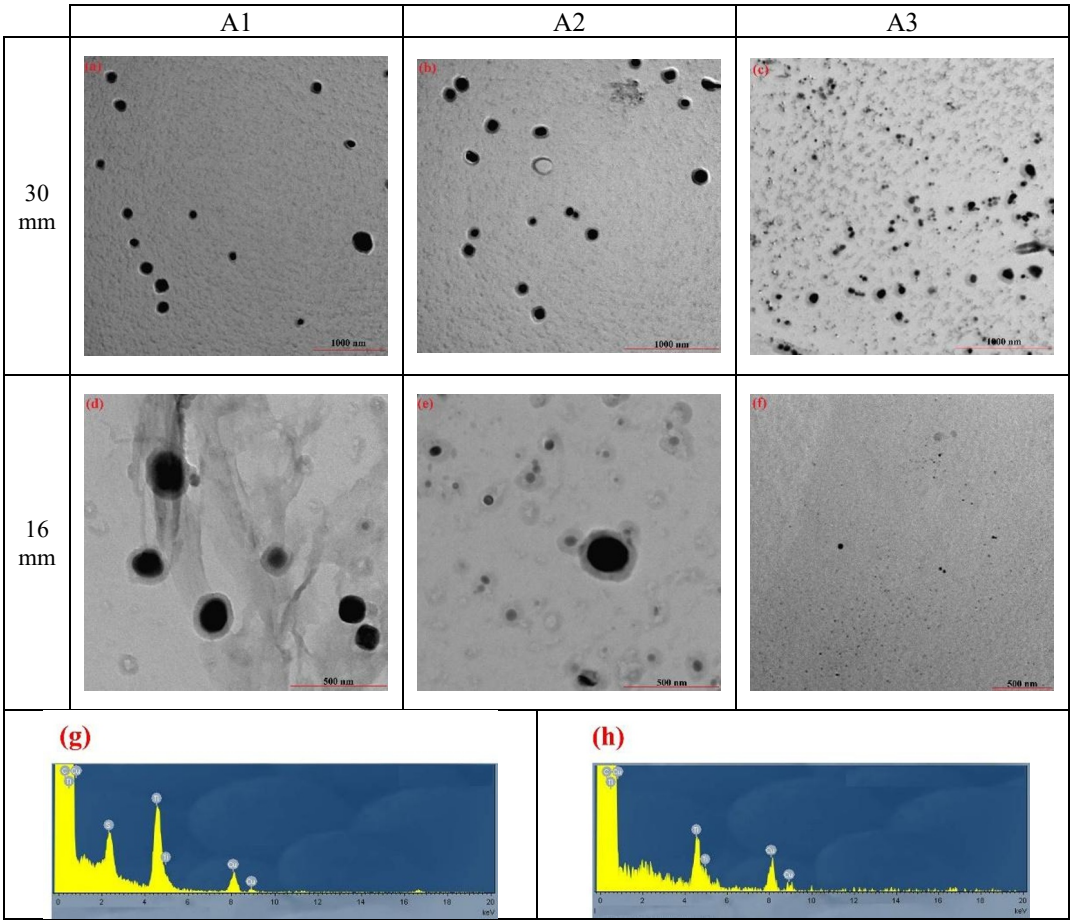

Fig. 6. TEM micrograph of precipitated and EDS spectra. Note that the magnification is different between 16- and 30-mm plate samples.

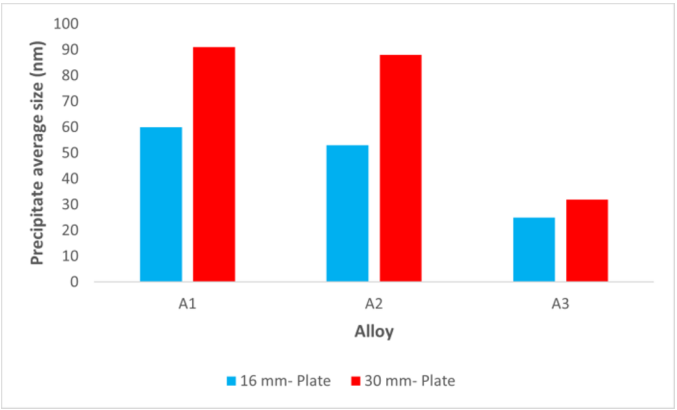

Fig. 7. A comparison of the average of precipitate sizes of the tested steels after cooling

3.3 Mechanical properties:

The hardness values of the tested steels are presented in Figure 8. Figure 9 (a) displays a schematic stress-strain curve for tested alloys, derived from the PIP test, and the variations in tensile properties as a function of cooling rate and alloy composition are illustrated in Figure 9 (b). Overall, an increase in the cooling rate led to higher hardness, yield strength (YS), and ultimate tensile strength (UTS). Improved mechanical performance was also observed with increasing carbon equivalent (Ceq) values. However, a comparison between A1 and A2, which had nearly identical Ceq values, revealed that doubling the vanadium content did not result in a notable change in mechanical properties. In HSLA steels with a high Ti content, most of the grain refinement and precipitation strengthening is already dominated by early-forming Ti-based precipitates such as TiN, and TiC. These precipitates control austenite grain size during hot working and contribute strongly to dislocation generation. When the V content is doubled in such compositions, its effect on mechanical properties remains limited, because V tends to precipitate later as VC or (Ti,V)C and often forms complex precipitates together with Ti. So, a large portion of V goes into Ti-rich precipitates, so its independent contribution to precipitation hardening is reduced. The improvement in the mechanical properties of the materials with increasing cooling rate can be attributed to grain refinement and precipitate size reduction. Additionally, the enhancement in mechanical performance with increasing carbon equivalent (Ceq) is associated with the formation of acicular ferrite and bainite.

The mechanical properties of HSLA steels are controlled by a combination of strengthening mechanisms, including grain refinement, precipitation hardening, solid-solution strengthening, and dislocation strengthening. Increasing the cooling rate during thermomechanical processing leads to the development of finer microstructures; most notably acicular ferrite (AF) in steels with a higher carbon equivalent (Ceq), which restricts dislocation motion through tightly interlocked grain boundaries and promotes higher dislocation densities, thereby improving strength and toughness. A faster cooling rate also reduces the average precipitate size while increasing their number density. The resulting population of finer, more closely spaced precipitates offers a greater interfacial area for dislocation pinning, enhancing the overall mechanical strength of the steel without a significant loss in ductility.

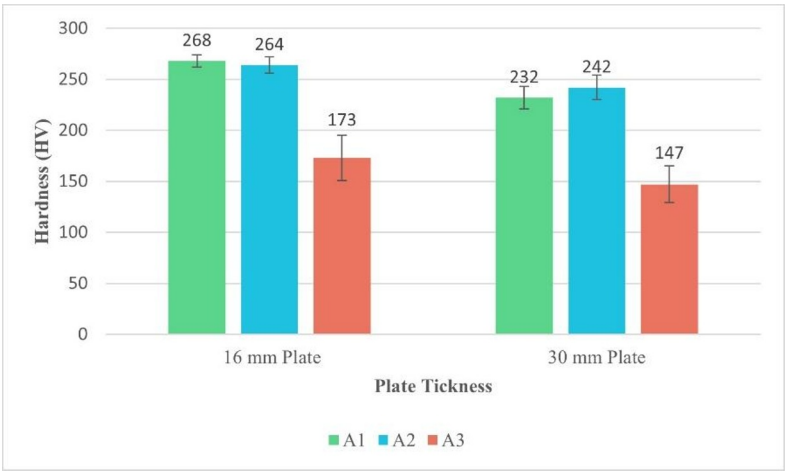

Fig. 8. Hardness of tested samples after cooling.

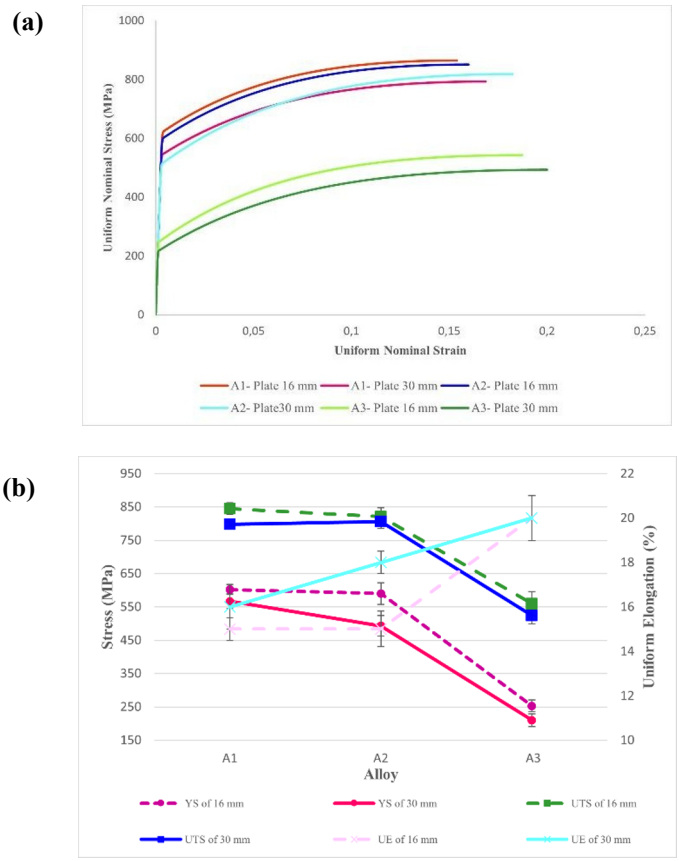

Fig. 9. (a) Plot of stress- strain curves, and (b) variation of mechanical properties.

4 Conclusions

In this study, the effects of cooling rate and alloy chemical composition on the microstructure and mechanical properties of Ti-V microalloyed steels were investigated. The key findings were summarized as follows:

- At low cooling rates, the microstructures primarily consisted of polygonal ferrite and pearlite. However, with increasing carbon equivalent (Ceq) and cooling rate, acicular ferrite and bainite formation were observed.
- The precipitation behavior and volume fraction of precipitates were found to be highly sensitive to the cooling rate. An increase in cooling rate led to a reduction in precipitate size.
- Precipitate size was also influenced by the alloy's chemical composition; specimens with lower C_{eq} values exhibited finer precipitates.
- It was observed that doubling the vanadium content had no significant impact on the mechanical properties within the investigated chemical composition range.

References

[1] "Climate Change & CO2," OICA, [Online]. Available: https://www.oica.net/category/climate-change-and-co2/. [Accessed 2017].

[2] P. T. Latake, P. Pawar and A. C. Ranveer, Int. J. Innov. Res. Creat. Technol., **1**, 333-337 (2015).

[3] M. Y. Demeri, Technology, and Application, (ASM International, Ohio, USA, 2013)

[4] P. Gong, E. Palmiere and W. Rainforth, Acta Mater.,**119**, 43-54 (2016).

[5] A. Zavdoveev, V. Poznyakov , T. Baudin, M. Rogante , H. S. Kim, M. Heaton , Y. Demchenko, V. Zhukov and M. Skoryk, Mat. Tod. Comm., **28**, 1-12 (2021).

[6] A. Qaban, T. Mohmed, M. Quazi and S. Naher, Mater. Today Commun., 25, 1-11 (2022).

[7] X. Wang, Z. C. Wang , X. B. Wang, Y. R. Wang, J. Q. GAO and X. L. ZHAO, J. Iron Steel Res., **19**, 62-66, (2012).

[8] J. G. Jung, J. S. Park, J. Kim and Y. K. Lee, Mater. Sci. Eng. A., **528**, 5529-5535 (2011).

[9] P. Gong, E. J. Palmiere and W. M. Rainforth, Acta Mater., **97**, 392-403 (2015).

[10] A. M. Elwazri, S. Yue and P. Wanjara, Metall. Mater. Trans. A., **36**, 2297-2305 (2005).

[11] V. V. Natarajan, V. S. A. Challa, R. D. K. Misra, D. M. Sidorenko, M. D. Mulholland, M. Manohar and J. E. Hartmann, Mater. Sci. Eng. A., **665**, 1-9 (2016).

[12] R. D. K. Misra, Z. Jia, R. O. Malley and S. J. Jansto, Mater. Sci. Eng. A., **528**, 8772-8780 (2011).

[13] B. Bhattacharya, S. Samanta, R. Ranjan and S. Ganguly, Ironmak. Steelmak., **0** (2024).

[14] F. Ma, G. Wen and W. Wang, Steel res. Int. , **84**, 1-7, (2013).

[15] M. Atkins, Atlas of continuous cooling transformation diagrams for engineering steels, (American Society for Metals, 1980).

[16] J. E. Campbel, H. Zhang, M. Burley, M. Gee, A. T. Fry, J. Dean and T. W. Clyne, Adv. Eng. Mater. , **23**, 1-13 (2021).

[17] J. Dong, C. Liu, Y. Liu, X. Zhou, Q. Guo and H. Li, Fusion Eng. Des., **125**, 423-430 (2017).

[18] D. Miao, H. Jiang, X. Cai, Z. Wang, J. Zhou and F. Xue, SSRN, 4570627 (2023)

[19] L. Yon, Mater. Sci. Technol., (2014).

[20] X. Zhang, C. loannidou, G. H. T. Gert H. ten Brink, A. N. López, J. Wormann, J. Campaniello, R. M. Dalgliesh, A. W. A. V. Well, S. E. Offerman, W. Kranendonk and B. J. Kooi, Mater. Des., **192**, 1-13 (2020).